Interaction Scheme and Temperature Behavior of Energy Transfer in a Light-Emitting Inorganic-Organic Composite System

ARTICLE *in* ADVANCED FUNCTIONAL MATERIALS · MARCH 2008

Impact Factor: 11.81 · DOI: 10.1002/adfm.200700538

4 AUTHORS, INCLUDING:

Antonio Alvaro Ranha Neves
Universidade Federal do ABC (UFABC)
51 PUBLICATIONS **505** CITATIONS
SEE PROFILE

Andrea Camposeo
Italian National Research Council
128 PUBLICATIONS **1,514** CITATIONS
SEE PROFILE

ADVANCED FUNCTIONAL MATERIALS

FULL PAPER

DOI: 10.1002/adfm.200700538

Interaction Scheme and Temperature Behavior of Energy Transfer in a Light-Emitting Inorganic-Organic Composite System**

By *Antonio Alvaro Ranha Neves, Andrea Camposeo, Roberto Cingolani,* and *Dario Pisignano**

Determining and controlling the inter-component excitation conversion in light-emitting nanocomposite materials is a key factor for predicting the composite luminescence properties and for the operation of many opto-electronic devices. Here we present an extensive study of the inter-component energy transfer in the composite system given by ZnO particles interacting with the conjugated polymer, poly[2-methoxy-5-(2-ethylhexyloxy)-1,4-phenylenevinylene]. The composite emission is studied upon varying the acceptor concentration, and the system temperature in the range 50–300 K. The temperature dependence of the energy transfer rate is described by a rate model, taking into account the temperature dependence of the single components nonradiative decay rates, and a dipole–surface interaction scheme in the hybrid material. The proposed model accounts very well for the experimental observation of energy transfer and can be used to predict the temperature behavior of the emission from light-emitting nanocomposite materials.

1. Introduction

Hybrid organic/inorganic nanocomposites are the subject of a fast growing area of research, since a lot of basic and practical interest has been raised by their optical properties, including broadly tunable photo- and electro-luminescence, photochromisms, photorefractivity, and nonlinear optical features.[1–7] Concerning the organic component of optically active nanocomposite materials, great attention has been given to conjugated polymers, due to their ease of processing and good opto-electronic characteristics. On the other hand, for the inorganic component, oxide and semiconductor micro- and nanocrystals are the most suitable media to provide homogeneous dispersion conditions and more effective charge transfer in the composite.

Although different light-emitting molecules can be blended to form emissive layers in organic-based photonic devices, inorganic-organic composite systems offer several advantages compared to purely polymeric blends, as they can also benefit from the inorganic component, being structurally and chemically more stable. From a basic point of view, inorganic-organic composites provide the possibility to observe new types of fundamental excitations, due to resonant mixing of Frenkel and Wannier exciton states.[8] To date, classes of devices based on inorganic-organic composite systems include visible[2] and infrared[3] monochromatic and white[4] light-emitting diodes, solid-state lasers,[1,7] photovoltaic devices[5] and photodiodes with enhanced photocurrent.[6]

The interactions between the inorganic and the organic phase within a nanocomposite can be mediated by radiative or nonradiative energy transfer, or both.[9,10] In particular, nonradiative energy transfer can be utilized as strategy for the non-optical excitation of a conjugated polymer in hybrid inorganic-organic composite systems. This phenomenon has been predicted and observed in inorganic-organic heterostructures, constituted by inorganic quantum wells interacting with amorphous conjugated polymer films.[10,11] According to the theory of nonradiative energy transfer, the donor (D) excited state is transferred to the acceptor (A) non-radiatively by long-range dipole–dipole interactions. The transfer rate depends on the overlap between the D emission and the A absorption spectra, and on the mutual distance, R, between the D and A particles. The Förster theory for dipole–dipole interaction predicts an energy transfer decay rate scaling as R^{-6}:[12]

$$k_{FRET} = k_D \left(\frac{R_0}{R}\right)^6. \quad (1)$$

In the previous expression, k_D is the decay rate of the photoluminescence (PL) of the D species in the absence of A, which is given by $k_D = k_{D,R} + k_{D,NR}$ (where $k_{D,R} = 1/\tau_{D,R}$ and $k_{D,NR} = 1/\tau_{D,NR}$ are the donor radiative and nonradiative decay rate respectively) and the Förster distance, R_0, is defined by:

$$R_0^6 = \frac{9000(\ln 10)\kappa^2 \Phi_D}{128\pi^5 N_{AV} n^4} \int_0^\infty I_D(\lambda)\varepsilon_A(\lambda)\lambda^4 d\lambda \quad (2)$$

In this equation N_{AV} is the Avogadro's number, κ^2 is the orientational factor related to the D and A dipole moments (an average value of 2/3 is generally used),[13] Φ_D stands for the

[*] Dr. D. Pisignano, Dr. A. A. R. Neves, Dr. A. Camposeo, Prof. R. Cingolani
NNL, National Nanotechnology Laboratory of Istituto Nazionale di Fisica della Materia-Consiglio Nazionale delle Ricerche
c/o Distretto Tecnologico ISUFI, Università del Salento
via Arnesano, 73100 Lecce (Italy)
E-mail: antonio.neves@unile.it

[**] We gratefully acknowledge the financial support from the Regional Strategic Project ''Ponamat'' and from the Italian Institute of Technology.

quantum yield of the D species in the absence of A, n is the average refractive index in the region of spectral overlap between the D normalized PL spectrum, $I_D(\lambda)$, and the A molar absorption coefficient, $\varepsilon_A(\lambda)$. In terms of the A:D relative concentration, c, by observing that $c \propto R^{-3}$, an equivalent expression of Equation 1 is: $k_{FRET} = k_D(c/c_2)^2$, where c_2 is a constant proportional to R_0^{-3}.[14] The Förster picture of the energy transfer predicts therefore an interaction transfer rate fully determined by the spectral properties of the single components (Equation 1). Hence, the knowledge of the absorption and emission properties of the single components should allow one to predict the resulting spectral features of the interacting composite system.

In blends, the nonradiative energy transfer process is particularly favored, since D–A pairs are distributed throughout the entire volume rather than in a layered heterostructure, thus resulting in a number of A molecules in close proximity of a D excitation.[10,15,16] However, in the case of conjugated polymers, because of the poorly defined separation among the chromophores and the exciton diffusion along the polymer chains, the Förster theory is often not able to properly describe the optical properties of composite materials.[12,17] For these systems, pioneering studies have reported on energy transfer rates scaling differently from the Förster dipole–dipole theory, evidencing a $k_{FRET}(R)$ behavior depending on the interaction geometry (dipole–dipole, dipole–surface, or surface–surface).[12,18,19] In particular, in the case of a dipole–surface interaction, $k_{FRET} = k_D(R_1/R)^3$ where $R_1 = \sqrt[3]{\pi\rho R_0^6/6}$ and ρ is the density of the donor bulk material,[12] or equivalently defining c_1 as a constant proportional to R_1^{-3}, $k_{FRET} = k_D(c/c_1)$.

Given that energy transfer mechanisms are crucial for the operation of many opto-electronic devices relying on nanocomposite materials, determining and controlling the inter-component excitation conversion is important to predict the composite luminescence properties, and to limit the possible emission quenching induced by energy transfer towards non-radiative decay channels. In this paper, we present an extensive study of the inter-component energy transfer and of the process efficiency in an inorganic-organic composite system. In particular, the temperature dependence of the energy transfer rate determining the resulting nanocomposite emission color is experimentally investigated and explained by a rate equation model, taking into account the temperature dependence of the D and A nonradiative decay rates. As a prototype system, we present ZnO particles interacting with the conjugated polymer, poly[2-methoxy-5-(2-ethylhexyloxy)-1, 4-phenylenevinylene] (MEH–PPV). We compare the classical dipole–dipole and dipole–surface interaction representations for this system, finding that the dipole–surface interaction results in a better fit to the experimental data. The proposed model, describing effectively the overall emission from the light-emitting nanocomposite, can be employed to predict the luminescence properties of hybrid inorganic-organic systems and their temperature behavior.

2. Results and Discussion

2.1. Determination of the Acceptor–Donor Interaction Scheme in the Composite

The wide-gap semiconductor, ZnO (D) was chosen as inorganic donor because of its exciton binding energy ~60 meV,[20] assuring remarkable and stable emission even at room temperature, which makes it very suitable for both photonic devices and biomedical applications.[20–22] Composite films were obtained by MEH-PPV (A), and ZnO sub-micrometer crystals. The light-emitting components were embedded in an optically inert matrix of poly(methyl methacrylate) (PMMA), aiming to reduce the formation of nonradiative recombination centers in the acceptor due to oxidation,[23] and to improve the overall photostability (molecular and crystal structures of the used materials displayed in Fig. 1). The D emission and the A absorption at room temperature are reported in Figure 2, being peaked at 382 and 428 nm, with linewidth (FWHM) of approximately 13 and 117 nm, respectively.

A scanning electron microscopy (SEM) picture of the ZnO microcrystals is displayed in Figure 3a. The typical particle sizes were found in the range 0.5–1.0 μm. Figure 3b shows a contact-mode atomic force microscopy (AFM) picture of the surface topography of the spin cast composite film, evidencing a uniform distribution of the ZnO crystals and the absence of large (>1 μm) aggregates of particles.

The PL spectra of the composite films with different acceptor:donor (A:D) relative content are displayed in Figure 4. Upon increasing the conjugated polymer concentration, the intensity of the emission from ZnO decreases, whereas that from MEH-PPV increases, due to the non-radiative energy transfer from the donor micro-crystals. The effective coupling between the donor and acceptor components through Förster transfer, also for amounts of A as low as a few percents, is evidenced in Figure 5, where we show the dependence of the relative PL intensity from the A molecules in the composite films, $\phi = \int I_A(\lambda)d\lambda / \int [I_A(\lambda) + I_D(\lambda)]d\lambda$, as a function of the relative A:D concentration. ϕ exhibits a non-linear trend, characterized by a rapid increase for relative concentrations up to 5%, and then by a saturation, with a maximum value around 0.9 for A:D = 40%. This behavior can

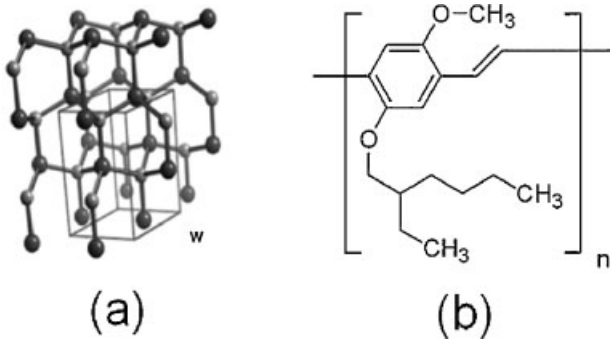

Figure 1. a) ZnO (donor) crystal structure (light dots = Zn atoms, dark dots = O atoms). b) MEH-PPV (acceptor) molecular structure.

ADVANCED FUNCTIONAL MATERIALS

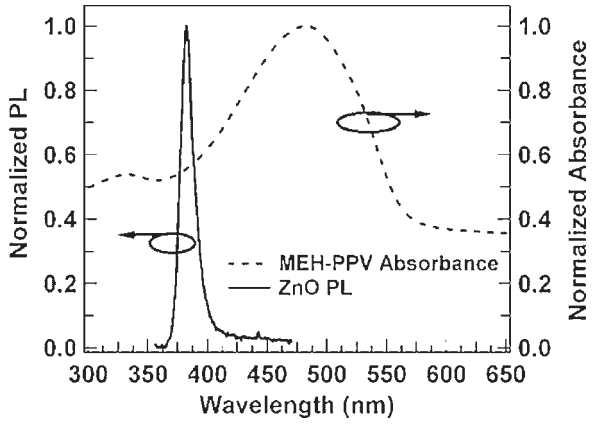

Figure 2. Normalized PL spectra of ZnO (continuous line, left axis) and absorbance of MEH-PPV (dashed line, right axis) at room temperature.

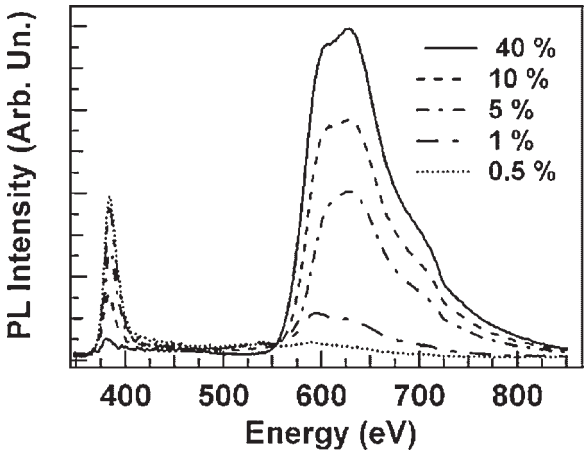

Figure 4. Emission spectra of the nanocomposites with different wt:wt A:D relative concentrations.

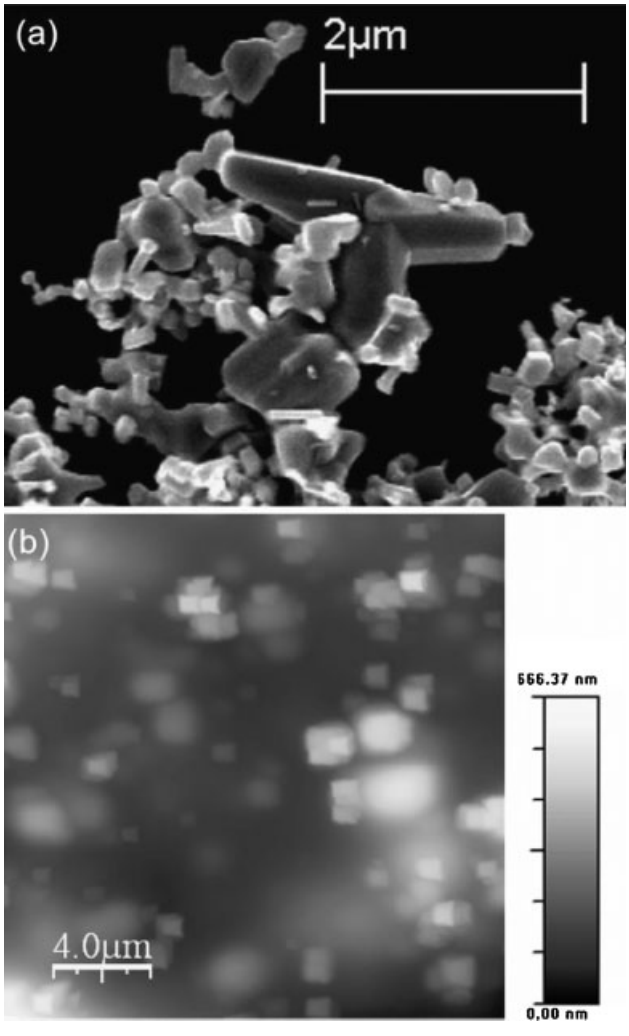

Figure 3. a) ZnO microparticles imaged by SEM. b) Surface topography of a hybrid film (A:D concentration 10%) imaged by AFM.

be rationalized by describing the energy transfer dynamics with the following rate equations for the populations, n_D (n_A) of D (A) in the excited state, also taking into account that a fraction of molecules of the conjugated polymer can be directly excited by incident photons:

$$\frac{dn_D}{dt} = f_D I - (k_D + k_{FRET}) n_D(t), \tag{3a}$$

$$\frac{dn_A}{dt} = f_A(c) I + k_{FRET} n_D(t) - k_A n_A(t). \tag{3b}$$

In the above expressions, $f_A(c)$ represents the fraction of pump flux, I (photons cm^{-3} s^{-1}), directly absorbed by a concentration, c, of A molecules, and f_D is the fraction absorbed by the donor population. The relative PL intensity

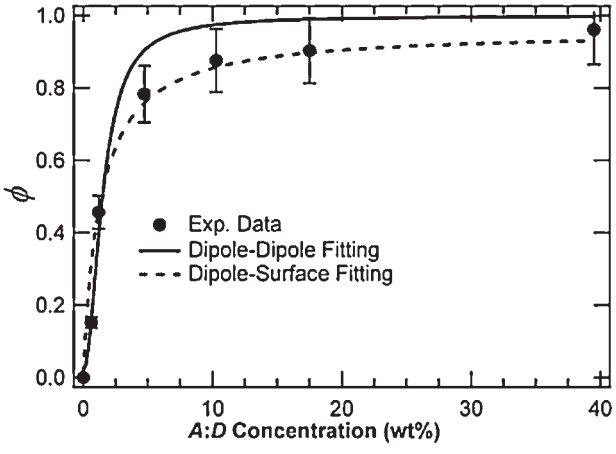

Figure 5. Integrated relative PL intensity, ϕ, from acceptors in the composite films vs. A:D relative concentration (dots). The superimposed curves are the best fits to the dipole–dipole (continuous line) and dipole–surface (dashed line) interaction models, respectively.

from the acceptor molecules is $\phi = k_{A,R}\, n_A/(k_{A,R}\, n_A + k_{D,R}\, n_D)$,[24] which, by solving Equation 3 for steady state, reads:

$$\phi = \left(1 + \frac{k_{D,R} n_D}{k_{A,R} n_A}\right)^{-1} = \left\{1 + \Phi_D \Big/ \Phi_A \left[\frac{f_A}{f_D} + \left(1 + \frac{f_A}{f_D}\right)\left(\frac{c}{c_p}\right)^p\right]\right\}^{-1}. \quad (4)$$

In the latter equation, Φ_D and Φ_A indicate the fluorescence quantum yield of the inorganic donor and of the organic acceptor, respectively and $p = 1$, 2, for the dipole–surface or dipole–dipole interacting components, respectively. We note that fitting Equation 4 to the experimental ϕ(A:D) data by a dipole–surface ($p = 1$) interaction provides a significantly better description of the experimental results as compared to the dipole–dipole scheme ($p = 2$) (Fig. 5). This result is attributed to the finite sub-micrometer size of the ZnO crystals, which is about 1–2 orders of magnitude larger than the typical MEH-PPV molecular size (1–10 nm).[25] Hence, the D–A pairs can be schematized as an infinite ZnO plane interacting with the MEH-PPV molecule dipoles. By the fit we could extract the value of the critical polymer concentration, c_1, which turns out to be (2.5 ± 0.1). In other words, for achieving a nonradiative energy transfer from the inorganic donor to the organic acceptor in the nanocomposite as efficient as the other decay channels of ZnO excitations, one needs an A:D relative concentration of the order of 2%.

2.2. Temperature Dependence of the Nonradiative Energy Transfer Rate

A better understanding of the nonradiative interaction occurring in the composite system can be achieved by analyzing the temperature dependence of the emission from both the single components and the blend film. To this aim, we first investigated the luminescence behavior of the inorganic donor and of the organic acceptor, then describing the nonradiative interaction in the nanocomposite material by a dipole–surface energy transfer model.

2.2.1. Inorganic Donor

The native PL spectra of ZnO microcrystals, embedded in a PMMA film, for different temperatures are shown in Figure 6a. Upon decreasing temperature, the ZnO emission spectra undergo a remarkable increase in intensity, a narrowing of the peak linewidths, and a blue-shift of the corresponding peak energies. Only above 150 K the thermal broadening of the transition linewidths determines the overlap of different emission peaks, preventing to distinguish the different transitions. At 50 K, the peaks at 3.36 eV (peak I_D in Fig. 6a), 3.31 eV (peak II_D) and 3.24 eV (peak III_D), attributable to bound excitons are instead clearly visible, together with a broad low-energy emission tail below 3.18 eV, which is due to the convolution of the LO-phonon replicas of

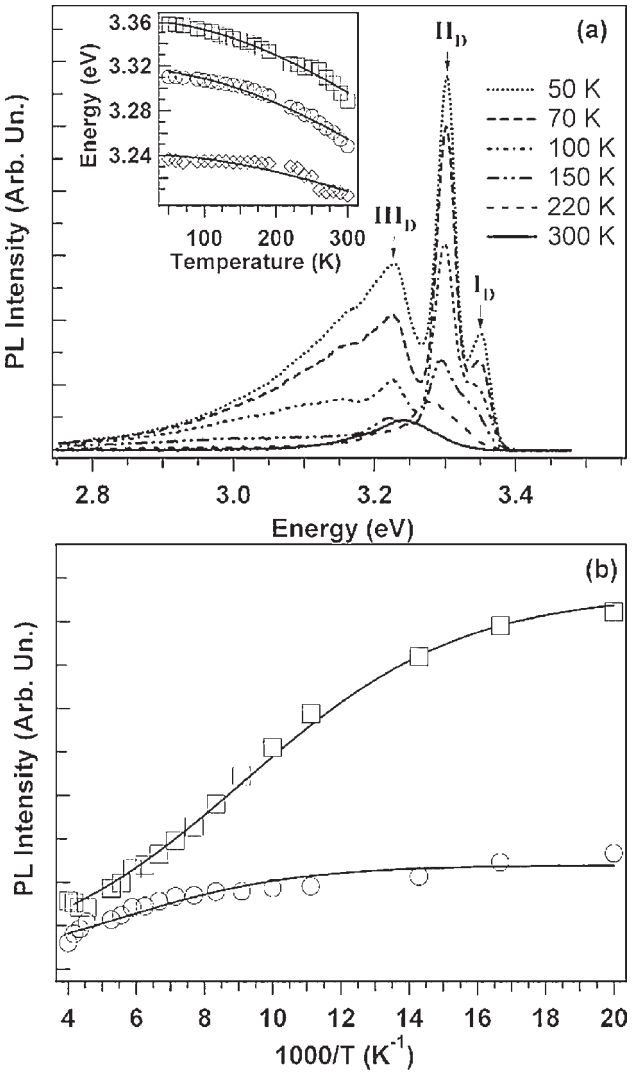

Figure 6. a) Emission spectra of ZnO microcrystals dispersed in a PMMA matrix as a function of temperature (from top to bottom 50, 100, 150, 210, and 300 K). The three peaks, I_D, II_D, and III_D, are indicated by the vertical arrows. Inset: Energies of the PL maxima as a function of temperature for the peaks I_D (squares), II_D (circles), and III_D (diamonds). Data fitted with Varshni law (superimposed lines). b) PL integrated intensity of the peaks I_D (squares) and II_D (circles) vs. temperature. The continuous line are the fits to the data by Equation 5.

the main transitions.[26–28] The band-gap narrowing resulting in the red-shift of the ZnO peak energies upon increasing temperature can be described by a Varshni's law,[29–31] $E_{ZnO}(T) = E(0) - \alpha T^2/(T + \theta_D)$, as showed in the inset of Figure 6a.

The plot of the intensity of the peaks I_D and II_D as a function of the inverse temperature, obtained by the deconvolution of the emission spectra by a multiple Gaussian fit, is displayed in Figure 6b. Upon increasing temperature, the emission intensity is quenched by thermally activated non-radiative recombination channels, characterized by a rate: $\tau_{NR} = \tau_0 \exp(E_a/kT)$, where E_a stands for the process activation

ADVANCED FUNCTIONAL MATERIALS

energy.[32] Under steady state, the intensity quenching can be consequently described by the expression:

$$I = I_0/[1 + C\exp(-E_a/kT)], \quad (5)$$

where $C = \tau_R/\tau_0$. This expression, valid under the assumptions of temperature-independent radiative lifetime and nearly-unity quantum efficiency at low temperature,[33] provides an activation energy of about 27 meV, which is comparable to that reported for bulk ZnO.[32]

2.2.2. Organic Acceptor

The PL spectra of a MEH-PPV film, measured at different temperatures and displayed in Figure 7, are composed by the vibronic replicas of the excitonic transition at 2.05 eV (at 50 K). Upon decreasing temperature, also for the organic component the emission intensity increases, due the quenching of the nonradiative decay processes, whereas in this case the peak energies undergo a red-shift (inset of Fig. 7a). The increase of the emission energies upon increasing temperatures can be associated to the decrease of the conjugation length in the polymer, due to torsional and liberation modes.[34] The integrated PL intensity as a function of the inverse temperature is displayed in Figure 7b. The data, fitted by Equation 5, indicate an activation energy of about 90 meV.[35]

2.2.3. Nanocomposite System

The PL spectra from ZnO:MEH-PPV composites with 10% A:D concentration, collected at temperature between 50 and 300 K, are shown in Figure 8. We observed that the composite basically retains the behavior of the constituent organic and the inorganic species upon varying temperature. The peak energy of the (0–0) exciton emission from the conjugated acceptor polymer exhibits a continuous blue-shift (from 2.02 to 2.07 eV) upon increasing temperature, whereas the ZnO bound exciton emission is concomitantly red-shifted from 3.29 to 3.24 eV. Similar results hold for each A:D concentration.

In order to have an insight into the temperature dependence of the energy transfer rate, we investigated the temperature behavior of the relative PL intensity from the A molecules (ϕ) for composites with different A:D relative concentrations (Fig. 9). Upon decreasing temperature, ϕ decreases by almost 50%, depending on the A:D relative concentration. The system temperature can affect the energy transfer rate through: (i) the D and A emission efficiency and decay rate (Φ_D and k_D) and, (ii) the critical concentration, c_1, via Equation 2, because of the possible variation of the spectral overlap between the D emission and the A absorption or the D fluorescence quantum yield. However, we did not observe significant variations in the overlap integral, $\int_0^\infty I_D(\lambda)\varepsilon_A(\lambda)\lambda^4 d\lambda$, by measuring the A absorbance and the D PL between 50 and 300 K. Consequently, the temperature dependence of the energy transfer has to be mainly related to changes in the D and A quantum efficiency and decay channels.

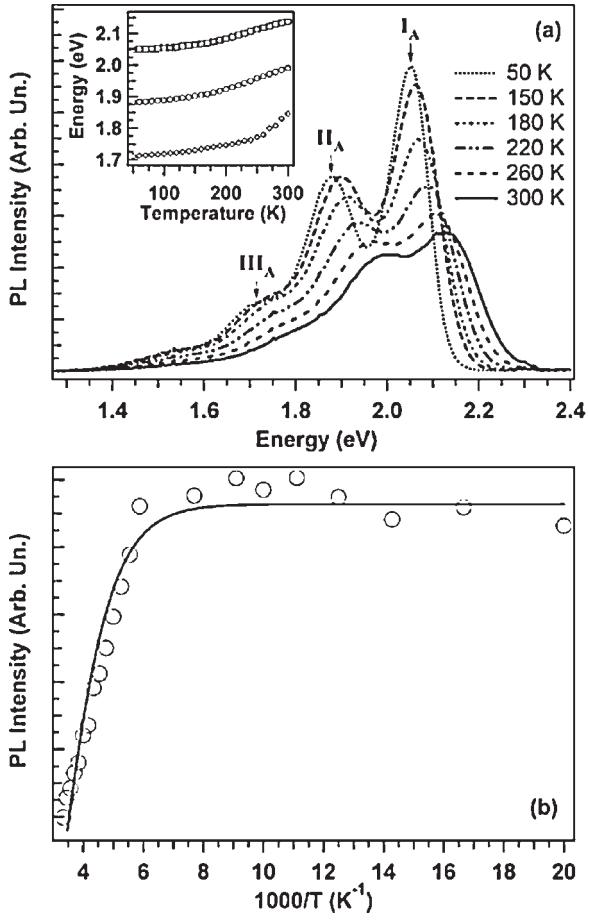

Figure 7. a) Emission spectra of MEH-PPV films as a function of temperature (from top to bottom: 50, 150, 180, 220, 260, and 300 K). The three peaks, I_A, II_A, and III_A, corresponding to the 0–0, the 0–1, and the 0–2 vibronic transitions, are indicated by the vertical arrows. Inset: Energies of the PL maxima as a function of temperature for the peaks I_A (squares), II_A (circles) and III_A (diamonds). b) PL integrated intensity vs. temperature. The continuous line is a fit to the data by Equation 5.

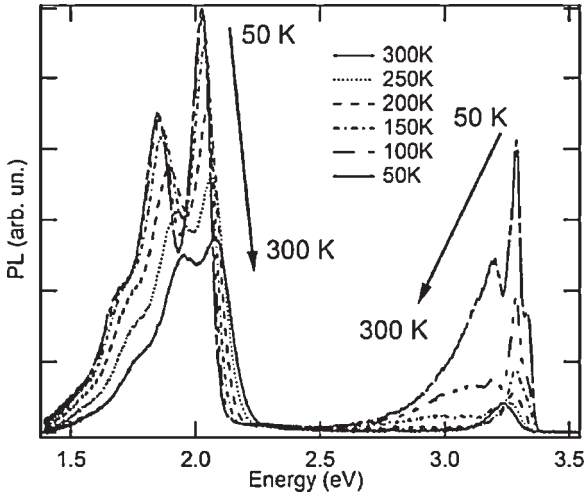

Figure 8. PL emission spectra (A:D 10 wt %) collected at different temperatures (from top to bottom, intervals of 50 K). The arrows indicate the acceptor blue-shift and donor red-shift upon increasing temperature.

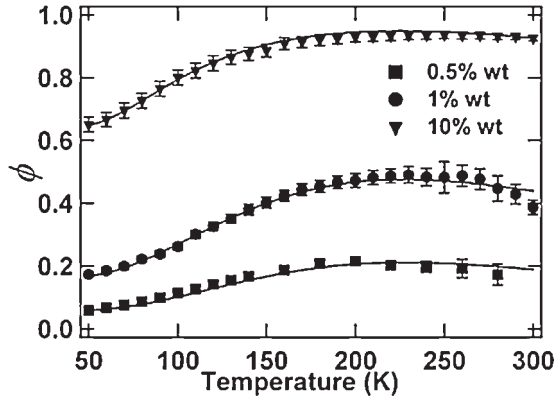

Figure 9. Temperature dependence of ϕ for different A:D concentrations. Points represent experimental data, whereas the superimposed curves represent the result of the modeling by Equation 4, taking into account the temperature dependence of the acceptor and donor recombination rates.

In particular, Equation 4 provides the expression for the temperature dependent nonradiative energy transfer, allowing us to model the experimental data reported in Figure 9.[36] By employing the values of the activation energies obtained from the data of Figure 6 and 7, and estimating the fraction of excited donor and acceptor species by absorption measurements on the composite system, we obtained for ϕ the temperature behavior displayed by the continuous lines in Figure 9. We found therefore that this model, taking into account the temperature dependence of both the donor and the acceptor nonradiative recombination rate, well describes the experimental findings, thus further validating the surface–dipole interaction scheme ($p=1$ in Equation 4) in the light-emitting nanocomposite. The good agreement between model and experimental data confirms that nonradiative energy transfer processes in hybrid inorganic-organic composites can be fully explained by a Förster-like description, by taking into account the necessary corrections for the different interacting geometries. The knowledge of the single components recombination processes, and of their temperature dependence, allowed us to determine the behavior of the composite. As a result of this analysis, a straightforward criterion to control the relative PL intensity of the acceptor component in light-emitting nanocomposites can be recognized, since the choice of donors with lower activation energies for nonradiative recombination channels increases the D–A energy transfer rate at room temperature, and consequently the yield from the acceptor molecule.[37]

3. Conclusions

We studied the dependence of the nonradiative energy transfer efficiency on temperature and on the relative concentration of acceptor and donor particles in a hybrid organic-inorganic composite system. We found that a dipole–surface interaction scheme properly describes the experimental data. In addition, the analysis of the temperature dependence of the emission from the inorganic and organic component allowed us to determine the characteristic activation energies of the nonradiative recombination rates that, inserted in the energy transfer rate equations, enable the prediction of the temperature dependence of the emission from the composite system. The quantitative understanding of these processes is crucial for the development of optimized hybrid organic/inorganic light-emitting devices, and lasers whose spectral emission rely on energy transfer in active nanocomposite media.

4. Experimental

ZnO microcrystals and MEH-PPV were purchased by Sigma-Aldrich and by American Dye Source Inc., respectively, and used as received without any further purification. Toluene solution were spin cast onto 1 cm^2 quartz substrates, obtaining films with MEH-PPV:ZnO (A:D) concentrations of 0, 0.5, 1, 5, 10, 20, 40% by weight, and uniform thickness of 1 μm, as measured by a step profilometer. To avoid degradation, the samples were stored in the dark and under vacuum before measurements. Absorption spectra were measured by a Cary 5000 (Varian) spectrophotometer. PL was excited by using a He-Cd laser emitting at 325 nm (spot size 1 mm^2) and an emitting power of 0.1 mW, chosen in order to avoid sample photo-degradation. Steady-state PL spectra were measured by using a fiber-coupled monochromator (Jobin Yvon) equipped with a charge coupled device detector (Jobin Yvon). For PL measurements at variable temperature (10–300 K), the samples were mounted in a He closed-cycle cryostat under vacuum (10^{-4} mbar). The emission from the sample surface was collected by a quartz lens with numerical aperture 0.17. All the experimental data were corrected for the instrumentation response.

Sample morphology was characterized both by scanning electron microscopy and atomic force microscopy. The AFM measurements were performed by exploiting a Veeco multimode head and a Nanoscope IIIa controller. The topographic images were obtained in contact mode using Si_2N_3 cantilevers (elastic constant 0.1 N m^{-1}).

Received: May 15, 2007
Revised: November 8, 2007

[1] C. Sanchez, B. Lebeau, F. Chaput, J. P. Boilot, *Adv. Mater.* **2003**, *15*, 1969.
[2] V. L. Colvin, M. C. Schlamp, A. P. Alivisatos, *Nature* **1994**, *370*, 354.
[3] N. Tessler, V. Medvedev, M. Kazes, S. Kan, U. Banin, *Science* **2002**, *295*, 1506.
[4] Y. Li, A. Rizzo, R. Cingolani, G. Gigli, *Adv. Mater.* **2006**, *18*, 2545.
[5] W. H. Huynh, J. J. Dittmer, A. P. Alivisatos, *Science* **2002**, *295*, 2425.
[6] N. Cho, K. R. Choudhury, R. B. Thapa, Y. Sahoo, T. Ohulchansky, A. N. Cartwright, K. S. Lee, P. N. Prasad, *Adv. Mater.* **2007**, *19*, 232.
[7] V. C. Sunder, H. J. Eisler, T. Dong, Y. Chan, E. L. Thomas, M. G. Bawendi, *Adv. Mater.* **2004**, *16*, 2137.
[8] V. Agranovich, R. Atanasov, F. Bassani, *Solid State Commun.* **1994**, *92*, 295.
[9] G. Heliotis, P. N. Stavrinou, D. D. C. Bradley, E. Gu, C. Griffin, C. W. Jeon, M. D. Dawson, *Appl. Phys. Lett.* **2005**, *87*, 103505.
[10] G. Heliotis, G. Itskos, R. Murray, M. D. Dawson, I. M. Watson, D. D. C. Bradley, *Adv. Mater.* **2006**, *18*, 334.
[11] D. Basko, G. C. La Rocca, F. Bassani, V. M. Agranovich, *Eur. Phys. J. B* **1999**, *8*, 353.

ADVANCED FUNCTIONAL MATERIALS

[12] J. Cabanillas-Gonzalez, A. M. Fox, J. Hill, D. D. C. Bradley, *Chem. Mater.* **2004**, *16*, 4705.
[13] L. M. Herz, C. Silva, R. H. Friend, R. T. Phillips, S. Setayesh, S. Becker, D. Marsitsky, K. Müllen, *Phys. Rev. B* **2001**, *64*, 195203.
[14] E. J. W. List, C. Creely, G. Leising, N. Schulte, A. D. Schlüter, U. Scherf, K. Müllen, W. Graupner, *Chem. Phys. Lett.* **2000**, *325*, 132.
[15] J. Liu, Y. Shi, Y. Yang, *Appl. Phys. Lett.* **2001**, *79*, 578.
[16] T. Q. Nguyen, I. B. Martini, J. Liu, B. J. Schwartz, *J. Phys. Chem. B* **2000**, *104*, 237.
[17] P. Andrew, W. L. Barnes, *Science* **2000**, *290*, 785.
[18] H. Kuhn, *J. Chem. Phys.* **1970**, *53*, 101.
[19] V. Bulovic, A. Shoustikov, M. A. Balbo, E. Bose, V. G. Kozlov, M. E. Thompson, S. R. Forrest, *Chem. Phys. Lett.* **1998**, *287*, 455.
[20] D. M. Bagnall, Y. F. Chen, Z. Zhu, T. Yao, S. Koyama, M. Y. Shen, T. Goto, *Appl. Phys. Lett.* **1997**, *70*, 2230.
[21] T. Makino, C. H. Chia, N. T. Tuan, Y. Segawa, M. Kawasaki, A. Ohtomo, K. Tamura, H. Koinuma, *Appl. Phys. Lett.* **2000**, *76*, 3549.
[22] A. B. Djurisic, Y. H. Leung, *Small* **2006**, *2*, 944.
[23] M. Yan, L. J. Rothberg, F. Papadimitrakopoulos, M. E. Galvin, T. M. Miller, *Phys. Rev. Lett.* **1994**, *73*, 744.
[24] E. J. W. List, C. Creely, G. Leising, N. Schulte, A. D. Schlüter, U. Scherf, K. Müllen, W. Graupner, *Chem. Phys. Lett.* **2000**, *325*, 132.
[25] J. K. Grey, D. Y. Kim, B. C. Norris, W. L. Miller, P. F. Barbara, *J. Chem Phys. B* **2006**, *110*, 25568.
[26] A. Teke, Ü. Özgür, S. Dogan, X. Gu, H. Morkoç, B. Nemeth, J. Nause, H. O. Everitt, *Phys. Rev. B* **2004**, *70*, 195207.
[27] F.-Y. Jen, Y.-C. Lu, C.-Y. Chen, H.-C. Wang, C. C. Yang, B.-P. Zhang, Y. Segawa, *Appl. Phys. Lett.* **2005**, *87*, 252117.
[28] V. A. Fonoberov, K. A. Alim, A. A. Balandin, F. Xiu, J. Liu, *Phys. Rev. B* **2006**, *73*, 165317.
[29] L. Wang, N. C. Giles, *J. Appl. Phys.* **2003**, *94*, 973.
[30] A. Teke, Ü. Özgür, S. Dogan, X. Gu, H. Morkoç, B. Nemeth, J. Nause, H. O. Everitt, *Phys. Rev. B* **2004**, *70*, 195207.
[31] Y. P. Varshni, *Physica* **1967**, *34*, 149.
[32] A. B. M. Ashrafi, N. T. Binh, B. P. Zhang, Y. Segawa, *J. Appl. Phys.* **2004**, *95*, 7738.
[33] M. Leroux, N. Grandjean, B. Beaumont, G. Nataf, F. Semond, J. Massies, P. Gibart, *J. Appl. Phys.* **1999**, *86*, 3721.
[34] F. Kong, X. L. Wu, G. S. Huang, R. K. Yuan, C. Z. Yang, P. K. Chu, G. G. Siu, *Appl. Phys. A* **2006**, *84*, 203.
[35] This value is generally known to be affected by the sample preparation method (solvent, film processing, solution concentration). See for instance: T. G. Bjorklund, S.-H. Lim, C. J. Bardeen, *J. Phys. Chem. B* **2001**, *105*, 11970.
[36] This approach does not take into account eventual effects of aggregation or phase separation of the blend components.
[37] As future development, the model could also take into account the role of the temperature dependence of the refractive index.